

# Comparison of Continuous-Wave and Micropulse Modulation in Retinal Laser Therapy

Jenny Wang,<sup>1</sup> Yi Quan,<sup>2</sup> Roopa Dalal,<sup>2</sup> and Daniel Palanker<sup>2,3</sup>

<sup>1</sup>Department of Applied Physics, Stanford University, Stanford, California, United States

<sup>2</sup>Department of Ophthalmology, Stanford University, Stanford, California, United States

<sup>3</sup>Hansen Experimental Physics Laboratory, Stanford University, Stanford, California, United States

Correspondence: Jenny Wang, Stanford University, 452 Lomita Mall, Stanford, CA 94035, USA; [jiwang2@stanford.edu](mailto:jiwang2@stanford.edu).

Submitted: February 2, 2017  
Accepted: August 17, 2017

Citation: Wang J, Quan Y, Dalal R, Palanker D. Comparison of continuous-wave and micropulse modulation in retinal laser therapy. *Invest Ophthalmol Vis Sci.* 2017;58:4722–4732. DOI:10.1167/iovs.17-21610

**PURPOSE.** Recent progress in retinal laser therapy has centered upon using thermal stress below damage threshold or selective destruction of targeted tissue layers as a stimulus for retinal repair. Temporal modulation, including micropulse, is thought to increase the selectivity of laser treatment, but has not been carefully analyzed. We measure and model the tissue response to continuous-wave (CW) and micropulse laser to evaluate the advantages and drawbacks of temporal modulation.

**METHODS.** Thresholds of ophthalmoscopic visibility, which indicates damage to photoreceptors, and fluorescein angiography (FA), indicating damage to retinal pigment epithelium (RPE), were measured with 577-nm laser in rabbits for duty cycles ranging from 3% to 100% (CW) and pulse envelopes of 20 and 200 ms. Heat shock protein (HSP) expression was measured in rats. Thresholds were compared to a computational model of tissue response based on the Arrhenius integral.

**RESULTS.** Damage to photoreceptors was defined by average power, regardless of the duty cycle, as predicted by the model. The average power for FA threshold was lower with 5% duty cycle than with CW laser by  $22 \pm 15\%$  for 200-ms and  $35 \pm 21.5\%$  for 20-ms envelopes, demonstrating some heat localization to RPE. The ratio of RPE damage threshold to HSP expression threshold was  $1.30 \pm 0.15$  and  $1.39 \pm 0.11$  for 20 ms at 5% duty cycle and CW, respectively.

**CONCLUSIONS.** Micropulse modulation with sufficiently short envelope and duty cycle can help reduce the spread of heat from the light-absorbing RPE and choroid. However, this localization does not benefit nondamaging retinal laser therapy, which is intended to avoid any cell death.

**Keywords:** retinal laser, nondamaging retinal therapy, photothermal therapy, micropulse modulation, temporal modulation, arrhenius

Nondamaging retinal laser therapy (NRT) is a promising paradigm for treating macular disorders, such as diabetic macular edema (DME),<sup>1,2</sup> chronic central serous chorioretinopathy (CSCR),<sup>3</sup> idiopathic macular telangiectasia (MacTel),<sup>4</sup> and others, without the tissue destruction and scarring associated with conventional laser photocoagulation. NRT is believed to work by triggering a cellular response to sublethal thermal stress in the retinal pigment epithelium (RPE) and possibly other layers, which helps to restore normal function to diseased tissue.<sup>4,5</sup> The major challenge of this approach is the proper calibration of laser parameters to deliver a sufficient amount of thermal stress to induce therapeutic effect without excessive heating, which can kill RPE cells, overlying neural retina, or underlying choroid. This calibration is complicated by patient-to-patient and spot-to-spot variations in pigmentation and ocular transparency, which define the fraction of laser power being converted into heat. To account for some of these factors, titration of laser parameters to produce a visible lesion is commonly performed in the periphery, and a predetermined conversion is used to translate those results to nondamaging therapeutic settings in the macula.<sup>4,6</sup>

One approach frequently used for subvisible or nondamaging therapy is the subthreshold diode micropulse (SDM) laser,

which delivers 100- to 300-ms-long bursts of micropulses 0.1 to 0.3 ms in duration, repeated at 500 Hz, using 810-nm wavelength.<sup>7</sup> While SDM has been interpreted in various ways in the literature,<sup>2</sup> the “True” implementation has the same aim as NRT: tissue treatment by thermal stress that produces no retinal damage. Recently, yellow wavelength (577-nm) lasers have also been used instead of near-infrared,<sup>8</sup> and a shorter envelope (20 ms) has been applied that enables pattern scanning.<sup>9</sup> Micropulses can confine the tissue response to pigmented layers by producing rapid temperature spikes in the light-absorbing RPE and choroid, while the transparent retina is heated gradually as a result of heat diffusion.<sup>10</sup> In this way, the laser-induced thermal stress can be produced more selectively in the RPE, such that even an excessive heating of RPE may still spare the neural retina. Despite its growing use for nondamaging therapy, there is a lot of confusion regarding the proper power settings for micropulse laser. Clinical studies utilize a wide range of treatment parameters, with duty cycles (ratio of the laser micropulse duration to its period, 2 ms) ranging from 5% to 15%, total pulse lengths from 20 to 300 ms, and disparate titration procedures producing inconsistent outcomes,<sup>11–13</sup> which are difficult to compare to one another or to continuous-wave (CW) laser. In several studies, titration is



neglected altogether, and a single parameter set is used for all patients,<sup>5,14</sup> assuming that a sufficiently wide therapeutic window is enabled by the micropulse laser.

In this study, we measure the extent to which micropulse modulation affects tissue response at duty cycles from 3% to 100% (CW) to facilitate comparison between clinical studies using different laser settings and to understand the advantages and drawbacks of such temporal modulation. We measure the thresholds of three clinically detectable damage endpoints while varying the duty cycle at two overall pulse envelopes of 20 or 200 ms. We also measure the threshold of heat shock protein (HSP) expression, an indicator of cellular response to laser-induced thermal stress below damage threshold.

One widely used tool for understanding the effect of heating is the Arrhenius model, which we and others have described previously.<sup>4,15-17</sup> This model assumes that hyperthermia denatures a critical cellular component at a rate quantifiable as a temperature-dependent chemical reaction. We hypothesize that different types of cellular response, such as HSP expression or cell death, are triggered at different levels of denaturation,<sup>18,19</sup> which is calculated by integrating the denaturation rate over the time of hyperthermia, as follows:

$$\Omega(\tau) = A \int_0^{\tau} e^{-\frac{E^*}{kT(t)}} dt \quad (1)$$

where  $A = 1.6 \times 10^{55} \text{ s}^{-1}$  and  $E^* = 340 \text{ kJ/mol}$ , based on previous experimental work.<sup>20</sup> The rate coefficient  $A$  was chosen to normalize the Arrhenius integral  $\Omega = 1$  value to the cell damage threshold. A study of HSP expression following laser heating in bioluminescent mice by Sramek et al.<sup>21</sup> indicated that HSP expression begins around  $\Omega_{\text{HSP}} = 0.1 \Omega_{\text{damage}}$ , which we adopt for our model calculations. Despite the simple formulation with only the rate coefficient  $A$  and activation energy  $E^*$  as fitting parameters, the Arrhenius integral-based estimates of tissue damage reasonably matched the retinal damage thresholds in rabbits within pulse durations ranging from 1 to 200 ms.<sup>20</sup> Our experimental evaluation of tissue effects with different duty cycles tests the validity of the Arrhenius model with modulation down to 0.1-ms durations and provides guidance on translation of the model predictions to clinical endpoints. It also tests the hypothesis that both HSP expression and cell death can be modeled using the same reaction rate parameters. In combination with a computational model of the laser-induced retinal heating, this Arrhenius integral formulation can be used to assess the width of the therapeutic window and optimal temporal modulation for nondamaging retinal therapy.

## METHODS

### In Vivo Study

All animal studies were performed in accordance with the ARVO Statement for the Use of Animals in Ophthalmic and Vision Research, with approval from the Stanford University Animal Institutional Review Board. A total of 12 Dutch-belted rabbits (Western Oregon Rabbit, Philomath, OR, USA) were used for lesion threshold measurements. The rabbits were anesthetized with ketamine hydrochloride (35 mg/kg) and xylazine (5 mg/kg). Pupil dilation was achieved by one drop each of 1% tropicamide and 2.5% phenylephrine hydrochloride. Topical tetracaine hydrochloride (0.5%) was used for local anesthesia. A Mainster wide-field retinal contact lens (OMRA-WF; Ocular Instruments, Bellevue, WA, USA) was used for laser treatment, with hydroxypropyl methylcellulose as the contact gel. The conversion of nominal (aerial) to retinal

beam size with the contact lens on the rabbit eye was determined to be 70% by comparing the laser pattern spacing on unfixed whole-mount retina samples to the nominal pattern spacing.

For HSP expression and live-dead assay, a total of 25 Long Evans rats (Charles River Laboratories, Wilmington, MA, USA) were used. Rats were anesthetized with ketamine hydrochloride (75 mg/kg) and xylazine (5 mg/kg). The pupil was dilated with one drop each of 1% tropicamide and 2.5% phenylephrine hydrochloride. Topical tetracaine hydrochloride (0.5%) was used for local anesthesia. A glass coverslip was used as a contact lens, with hydroxypropyl methylcellulose as the contact gel. The demagnification of the rat eye with a coverslip was determined to be 45% by measuring laser pattern spacing on unfixed whole-mount retina and comparing it to the nominal pattern spacing.

### Laser Treatment and Evaluation

A 577-nm laser (Genesis MX577; Coherent, Inc., Santa Clara, CA, USA) was modulated at 500 Hz with duty cycles from 3% to 100% (CW) and overall pulse envelope of either 20 or 200 ms. Laser spots at 200- $\mu\text{m}$  setting (140  $\mu\text{m}$  on rabbit retina due to 70% demagnification) were delivered through a slit lamp. High-power marker burns were delivered first to outline the experimental grid. For damage threshold assessment, test spots were delivered at various power levels for 3%, 5%, 9%, 15%, 25%, 47%, and 100% duty cycles with 20- and 200-ms pulse envelopes. The number of spots for each setting is listed in Supplementary Table S1.

Lesions were given a binary visible/invisible grade for each of three tissue response levels: ophthalmoscopic visibility of the lesion, which is indicative of photoreceptor damage, (1) immediately (within 3 seconds) after laser delivery, (2) delayed by 1 to 5 minutes, and (3) visibility in fluorescein angiography (FA), which indicates damage to RPE. Fluorescein angiography was performed immediately after all the test spots were delivered in both eyes (between 1 and 2 hours after the first lesion). Fluorescein (0.2 mL, AK-FLUOR 10%; Akorn, Lake Forest, IL, USA) was injected in the marginal ear vein and imaging was performed using a scanning laser ophthalmoscope (Spectralis, Heidelberg Engineering, Heidelberg, Germany). The binary data on immediate ophthalmoscopic visibility (IV), delayed ophthalmoscopic visibility (DV), and FA visibility were fit to a probit model (statsmodels 0.6.1); and the LD50 point, 50% probability of a lethal dose, was used as the threshold.

To combine data across rabbits, we had to account for variation in pigmentation and ocular transparency between animals. For this purpose, DV thresholds with CW laser in each animal were first averaged across all subjects, yielding overall mean thresholds of  $53 \pm 8$  and  $26 \pm 5$  mW for 20 and 200 ms, respectively. Then, a normalization constant, representing the deviation of pigmentation and ocular transparency from average, was calculated for each animal by dividing the individual DV threshold by the overall mean DV threshold power. To normalize the data in each animal, experimental power values for all duty cycles and tissue response levels were divided by normalization constant. The experimental thresholds represent the LD50 points from probit fits to the combined, normalized data.

For HSP expression, laser spots of 90  $\mu\text{m}$  on the rat retina (45% demagnification of 200- $\mu\text{m}$  spot) were delivered through a slit lamp. First, high-power marker burns were placed to outline an experimental grid. Then, test spots were used to determine the IV threshold. Finally, experimental spots (30% to 80% of IV) were delivered in a grid to determine the cytotoxicity and HSP thresholds. Each experimental spot was given a binary grade for viability (live or dead) or HSP

TABLE 1. Parameters of the Model of Posterior Rabbit Eye, With Ocular Transparency of 55% for 577 nm

Tissue Layer	Thickness, $\mu\text{m}$	Absorption Coefficient $\mu_a$ , $\text{cm}^{-1}$ , for 577 nm	Scattering Coefficient $\mu_s$ , $\text{cm}^{-1}$ , for 577 nm	Anisotropy, g	% of Energy Incident on Retina Absorbed
Retina	112	5.23	333	0.97	6.6
RPE melanosomes	1	4200	4500	0.84	35.9
RPE basal layer	3	0	0	NA	0
Choriocapillaris	20	200	1600	0.94	22.1
Pigmented choroid	20	1050	1600	0.94	28.9
Nonpigmented choroid	30	200	1600	0.94	1.3

expression (present or absent). The data were combined across animals by expressing laser power as a percentage of the IV threshold, and the damage and HSP expression thresholds were calculated as the LD50 and ED50 (50% effective dose) points of probit model fits.

In each rat, one eye was used for HSP expression only, while the other eye was stained first for cellular viability, followed by immunofluorescence analysis of HSP expression (see Supplementary Materials for immunofluorescence protocol). Eyes were enucleated at 6 to 18 hours after laser delivery for HSP expression analysis and at 2 to 6 hours for damage threshold determination. The anterior segment of the globe was removed and the retina was peeled off the RPE. For cell viability assessment, the RPE-choroid-sclera sample was incubated with Calcein AM/EthD-III viability/cytotoxicity stain (Biotium, Fremont, CA, USA) for 30 minutes before washing and imaging with a fluorescence microscope. After imaging, these samples were further processed for measurement of HSP expression. Immunostained samples were imaged with a fluorescence microscope immediately after washing and mounting. Selected laser lesions were further imaged with a confocal microscope (Zeiss LSM 780; Carl Zeiss Microscopy, LLC., Thornwood, NY, USA).

**Computational Model**

Axisymmetric models of laser heating and tissue response for the rabbit and human eye were constructed in the finite element analysis package COMSOL5.2a (COMSOL, Burlington, MA, USA). Laser beam absorption profiles were calculated using the Monte Carlo Simulation Package (MCML, CONV) for photon transport in multilayered tissues.<sup>22,23</sup> The thicknesses and optical coefficients of the retinal and choroidal layers were taken from a previously described 577-nm rabbit model<sup>4,20</sup> with a few modifications. First, the RPE was divided into a highly absorbing and scattering layer representing the apical surface where the pigment-filled melanosomes are localized<sup>24</sup> and a transparent basal layer. The absorption and scattering coefficients were correspondingly modified to keep the total attenuation in the RPE the same. An ocular transparency term was introduced to account for loss of laser power in the contact lens and anterior segment prior to reaching the retina. To fit our experimental data, this was set

to 55% for 577 nm in a rabbit model. Second, a simplified human model was created for 810-nm laser irradiation using retinal, RPE, and choroidal thickness data from the literature.<sup>25-27</sup> The ocular transparency at 810 nm was assumed to be 65%, based on lower scattering at the longer wavelength. Optical coefficients for each layer were taken from Hammer et al.<sup>28</sup> and rescaled to match the clinical reports of damage and nondamage with 810-nm laser.<sup>7</sup> Light that was not absorbed in the retinal and choroidal layers (either backscattered or transmitted) was ignored in calculation of tissue heating. Geometric and optical parameters used in the rabbit and human models are summarized in Tables 1 and 2, respectively. The tissue thermal properties were assumed to be identical to those of water.

To estimate tissue response, an Arrhenius damage integral  $\Omega(\tau) = A \int_0^\tau e^{-\frac{E^*}{RT(t)}} dt$  was calculated with constants  $E^* = 340$  kJ/mol,  $A = 1.6 \times 10^{55} \text{ s}^{-1}$ ,  $R_{\text{gas}} = 8.3145$  J/mol-K for each point in space.<sup>20</sup> To correlate the Arrhenius integral distribution  $\Omega(r, z, \tau)$  to the experimental damage thresholds, we established correlation points at which  $\Omega_{\text{damage}}$  would have to be reached to produce a lesion. This approach was designed to exactly match our experimental CW measurements, so that the model predictions for micropulse would then reflect the deviation from our null hypothesis: that tissue response is defined by average power, regardless of duty cycle. First, we computed the Arrhenius integral distribution with the FA threshold power for 20-ms CW exposures and derived the correlation radius for visible lesions by solving  $\Omega(r_{\text{VIS}}, z_{\text{RPE}}, 20\text{ms}) = \Omega_{\text{damage}, 20\text{ms}} = 1$ , which yielded  $r_{\text{VIS}} = 60 \mu\text{m}$ . Here, we take  $z_{\text{RPE}} = -0.5 \mu\text{m}$  from the top of the RPE, in the middle of the RPE melanosome-rich layer. Calculations of the Arrhenius distribution for the FA threshold power with 200-ms CW at the same radius resulted in a slightly higher Arrhenius value:  $\Omega(60 \mu\text{m}, z_{\text{RPE}}, 200\text{ms}) = \Omega_{\text{damage}, 200\text{ms}} = 3.04$ . To estimate IV and DV thresholds, we assumed the same correlation radius and solved for the height above the RPE needed for immediate and delayed visibility at 20 and 200 ms:  $z_{\text{IV}20\text{ms}}$ ,  $z_{\text{DV}20\text{ms}}$ ,  $z_{\text{IV}200\text{ms}}$ , and  $z_{\text{DV}200\text{ms}}$ . For example, with the IV threshold power from 20-ms CW exposure, calculations yield  $z_{\text{IV}20\text{ms}} = 22.2 \mu\text{m}$  above the RPE for  $\Omega(r_{\text{VIS}}, z_{\text{IV}20\text{ms}}, 20 \text{ms}) = 1$ . The remaining correlation heights were  $z_{\text{DV}20\text{ms}} = 5.7 \mu\text{m}$ ,  $z_{\text{IV}200\text{ms}} = 29.5 \mu\text{m}$ , and  $z_{\text{DV}200\text{ms}} = 10.6 \mu\text{m}$ , as depicted in Figure 1. After

TABLE 2. Parameters of the Model of Posterior Human Eye, With Ocular Transparency of 66% for 810 nm

Tissue Layer	Thickness, $\mu\text{m}$	Absorption Coefficient $\mu_a$ , $\text{cm}^{-1}$ , for 810 nm	Scattering Coefficient $\mu_s$ , $\text{cm}^{-1}$ , for 810 nm	Anisotropy	% of Energy Incident on Retina Absorbed
Retina	272	0.26	0.95	0.97	1.1
RPE melanosomes	5	76	3000	0.84	6.8
RPE basal layer	10	0	0	NA	0
Choroid, undifferentiated	275	9.5	433	0.94	31.3

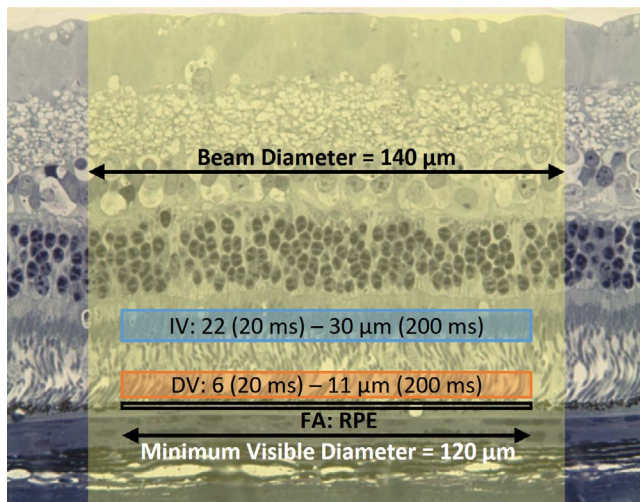


**FIGURE 1.** Parameters of the computational model for correlation to various clinical endpoints. The correlation diameter for a visible lesion in fluorescein angiography (FA), delayed ophthalmoscopic visibility (DV), or immediate ophthalmoscopic visibility (IV) is 120 μm. Correlation heights are shown for DV and IV in the shaded orange and blue boxes relative to RPE for 20- and 200-ms pulse durations.

establishing the damage integral values and correlation points based on experimental CW thresholds, the model was used to predict the same three thresholds for the other duty cycles. To estimate the window for nondamaging therapy, we assumed  $\Omega_{HSP} = 0.1 \Omega_{damage}$  based on Sramek et al.,<sup>21</sup> such that the therapeutic window for nondamaging therapy can be calculated as  $0.1 < \Omega_{20ms} < 1$  and  $0.304 < \Omega_{200ms} < 3.04$  for any point in the retina.

**RESULTS**

**Experimental Results**

Laser spots in rabbits were evaluated by three methods: IV, DV, and FA. The peak power thresholds for these three responses are plotted (filled circles) against duty cycle for 200 and 20 ms in Figures 2A and 2B, respectively. Error bars around each data point represent the 10% and 90% damage probability points (LD10-LD90) from the probit fit. The dotted lines show the peak powers corresponding to an average power (peak power multiplied by duty cycle) equal to the CW threshold. These lines represent the null hypothesis where micropulse modulation has no effect, so that only the average power defines tissue response. The solid lines show model predictions, which are discussed in the following section.

The IV and DV experimental thresholds fall very close to the dotted, constant-average-power lines at both 200 and 20 ms. This indicates that in the 5% to 100% duty cycle range, modulation does not significantly affect any of the ophthalmoscopic visibility damage thresholds. Only at the most extreme micropulse condition, 3% and 20 ms, did we observe a decrease in thresholds by 24% and 23% for immediate (IV) and delayed (DV) visibility, respectively. In contrast, the FA thresholds, which are indicative of damage to RPE cells, do show the effect of micropulse modulation with a significant deviation beginning below 9% duty cycle for 200 ms and below 15% for 20 ms.

HSP expression was observed in the rat RPE-choroid in two forms. The first is expression in the RPE cells themselves, as shown in Figures 3A and 3B in a damaging burn, where the red fluorescence indicating HSP expression matches the cell shape outlined by the zonula occludens-1 (ZO-1) marker in green. The second is expression beneath the RPE cell layer, in the choroid, which is present in damaging burns and predominant in nondamaging burns, as shown in Figure 3C. The cross-

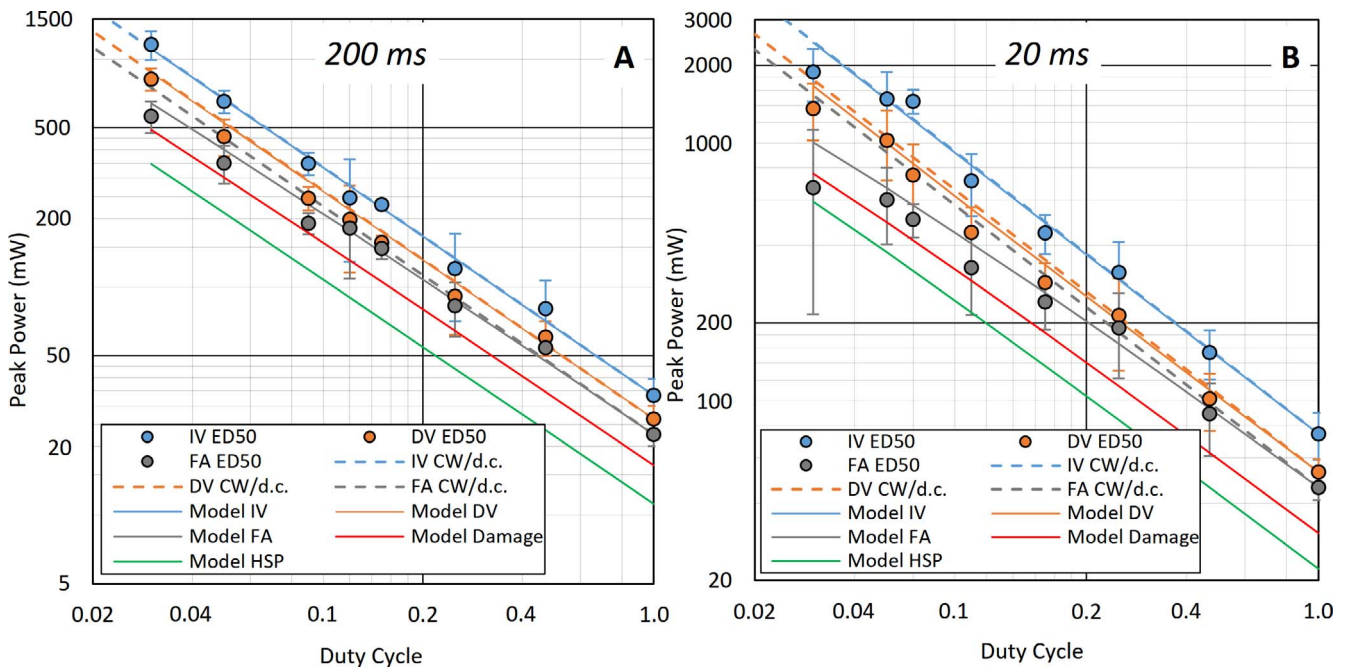


**FIGURE 2.** Log-log plots of experimental and model damage thresholds for 577-nm wavelength in rabbit, as a function of duty cycle with (A) 200-ms and (B) 20-ms overall pulse duration in 140-μm spot. Filled circles indicate experimental (LD50) damage thresholds evaluated by immediate ophthalmoscopic visibility (IV, blue), delayed visibility (DV, orange), and fluorescein angiography (FA, gray). Error bars show the LD10 to LD90 range. Dotted lines show the peak power corresponding to the constant average power relationship, while solid lines show the IV, DV, FA, single-cell damage, and HSP expression thresholds computed by the model.

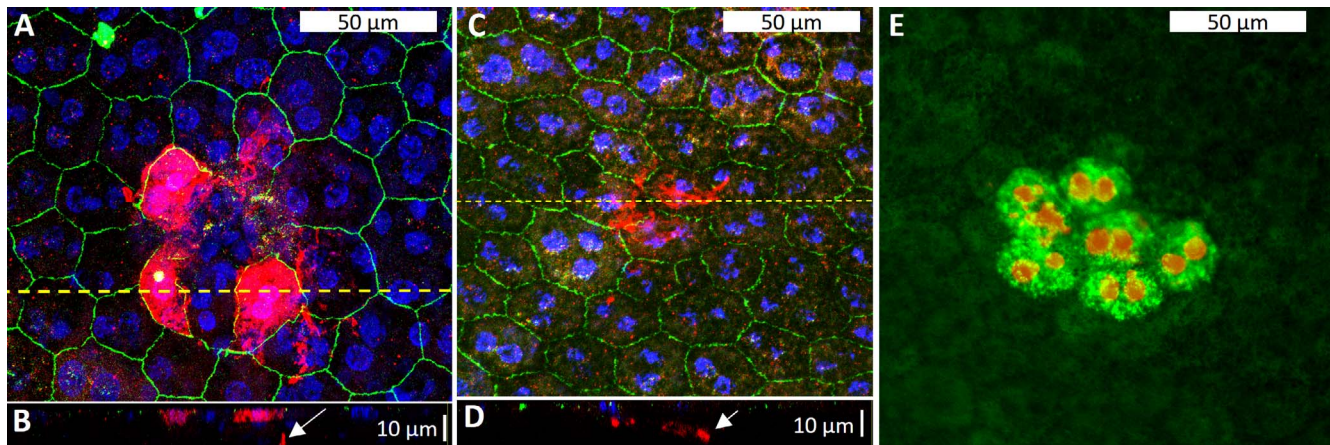


**FIGURE 3.** HSP70 expression and cell damage in the rat RPE. (A) Maximum-intensity projection of confocal micrograph after immunostaining of a damaging laser burn using 200 ms, 5% duty cycle, at 88% of titration power. Nuclei labeled *blue* 4',6-diamidino-2-phenylindole (DAPI), RPE cell outlines labeled *green* (ZO-1), and HSP70 labeled *red*. (B) Cross section of (A) along the *yellow dashed line*. *White arrow* indicates choroidal staining. (C) Maximum-intensity projection of confocal micrograph of immunostaining after nondamaging laser burn using 200 ms, 5% at 44% of titration power. (D) Cross section of (B). (E) Fluorescence micrograph of RPE after viability/cytotoxicity staining with dead nuclei in *red*.

sectional views in Figures 3B and 3D confirm that the choroidal HSP expression (white arrows) is below the RPE cell layer. To calculate the threshold for HSP expression, each lesion was given a binary grade for the presence or absence of HSP expression regardless of location, and a probit fit was calculated for expression versus power relative to IV threshold in that eye. Cytotoxicity staining was used to identify cell damage, where red fluorescent nuclear staining of the RPE, as in Figure 3E, was the indicator of damage, and a probit fit was calculated for damage versus power relative to IV threshold. This was measured for four settings: (1) 200 ms, CW, (2) 200 ms, 5% duty cycle, (3) 20 ms, CW, and (4) 20 ms, 5% duty cycle, and the threshold results are shown in Table 3.

**Computational Results**

The rabbit model for 577-nm wavelength was used to predict temperature rise and tissue response for comparison to experimental results. First, the temperature rise at each point in the tissue model was calculated as shown in Figure 4, overlaid on rabbit retinal histology. Then, the temperature at each point in space and time was used to calculate the local Arrhenius rate, which was then integrated over time, yielding the Arrhenius integral  $\Omega$ . Figure 5 shows the temperature course, Arrhenius rate, and integral  $\Omega$  at the minimum visible lesion radius on RPE, for the FA thresholds with CW laser and with 5% duty cycle (see also Supplementary Videos S1-S6). Although the temperature time courses are quite different, the Arrhenius integral at the FA correlation point is the same, and thus the tissue response is also hypothesized to match.

Using this method, predictions for the IV, DV, and FA threshold powers were made for duty cycles less than 1, as

shown by the solid blue, orange, and gray lines in Figure 2. Since the correlation between Arrhenius integral and tissue response was calibrated on the CW values, each line matches the experimental point exactly at CW. From there, the model reproduces much of the experimentally observed change with duty cycle: (1) IV and DV thresholds show negligible deviation from the constant-average-power lines, as experimentally observed, and (2) FA thresholds are slightly reduced compared to CW level with sufficiently low duty cycle for both 200 and 20 ms. Figure 2 also shows the predicted curves for the onset of HSP expression as well as the threshold for cellular damage, defined as  $\Omega_{HSP} = 0.1$  and  $\Omega_{damage} = 1$  for 20-ms pulse envelope and  $\Omega_{HSP} = 0.304$  and  $\Omega_{damage} = 3.04$  for 200 ms. From these predictions, the ratio of the damage threshold to IV lesion drops from 41% for CW to 33% for 5% duty cycle at 20 ms, and from 49% (CW) to 45% (5% duty cycle) for 200 ms.

Figure 6 demonstrates cross sections of  $\Omega$  in the rabbit model at the FA threshold with CW, 15%, and 5% duty cycle, for 20- and 200-ms pulse envelope. Similar cross sections for an ideal NRT treatment, which stops just below the onset of cellular damage, are shown in Figure 7. There are two clear trends: Decreasing the duty cycle increases (1) axial localization of the heat to the light-absorbing RPE and (2) lateral uniformity of the effect in the RPE plane, particularly with 20-ms pulse envelope, because heat diffusion is reduced during shorter pulses. At the FA threshold, 5% modulation with 20-ms envelope confines the damage zone to the volume just around the RPE and choroid (Fig. 6A, right). Therefore, micropulse modulation can help selectively damage the RPE while sparing the surrounding tissues. However, since no cells should reach the damage threshold for ideal NRT treatment (Fig. 7), micropulse modulation actually reduces the volume of HSP

**TABLE 3.** Thresholds of Damage and HSP Expression in Rat Eye After 577-nm Laser Treatment in 90- $\mu$ m spot. Error Is Given as the 95% Fiducial Limits to the 50% Probability of Damage or Expression

Settings	Immediately Visible Titration, Average Power	Damage Threshold, % of IV Threshold	HSP Expression Threshold, % of IV Threshold	Damage/HSP Therapeutic Window
200 ms, CW	18.2 $\pm$ 3.3 mW	64% $\pm$ 3	47% $\pm$ 3	1.36 $\pm$ 0.14
200 ms, 5% duty cycle	16.0 $\pm$ 1.1 mW	60% $\pm$ 3	43% $\pm$ 2	1.40 $\pm$ 0.15
20 ms, CW	28.9 $\pm$ 2.2 mW	68% $\pm$ 2	49% $\pm$ 2	1.39 $\pm$ 0.11
20 ms, 5% duty cycle	27.9 $\pm$ 3.1 mW	57% $\pm$ 3	44% $\pm$ 3	1.30 $\pm$ 0.15

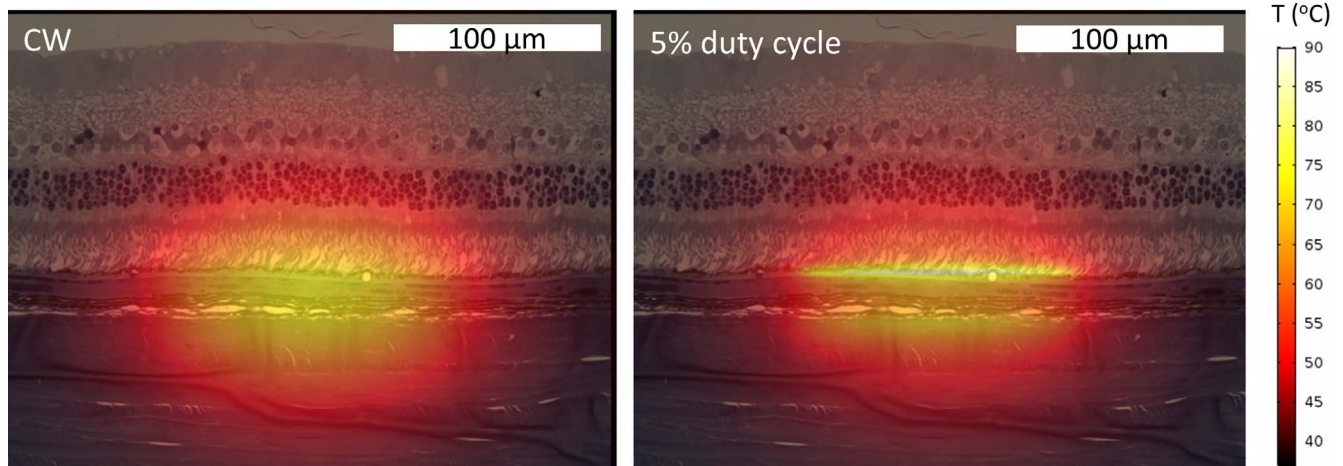


FIGURE 4. Computed temperature in the rabbit eye during 577-nm laser treatment with 140- $\mu\text{m}$  spot diameter for CW (left) and 5% duty cycle (right) over 20 ms at the modeled FA threshold power of 46 and 33.3 mW, respectively. Temperatures shown for 18.1 ms after beginning of the pulse.

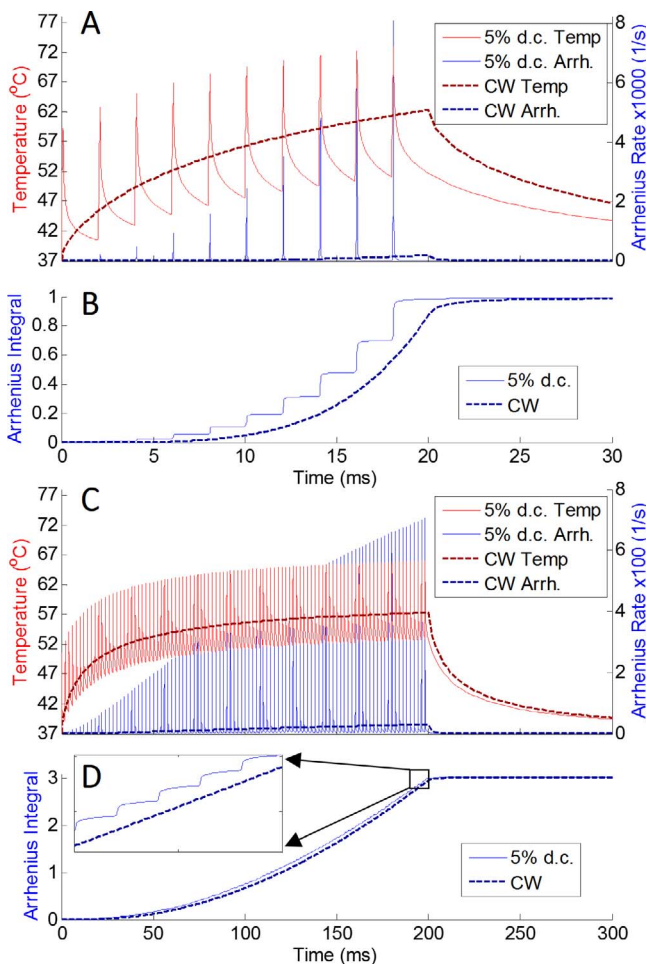


FIGURE 5. (A) Computed temperature (red) and Arrhenius rate (blue) at the minimum FA lesion radius of 60  $\mu\text{m}$  in the rabbit eye during 577-nm laser treatment with 20-ms pulse envelope with average power of 46 mW for CW and 33.3 mW for 5% duty cycle. (B) Arrhenius integral for the temperature course shown in (A). (C) Temperature and Arrhenius rate at minimum FA lesion radius of 60  $\mu\text{m}$  with 200-ms pulse envelope with average laser power of 22.6 mW for CW and 20.1 mW for 5% duty cycle. (D) Arrhenius integral for the temperature course shown in (C).

expression for a single laser spot from  $3.55 \times 10^{-4} \text{ mm}^3$  at CW to  $1.52 \times 10^{-4} \text{ mm}^3$  at 5% duty cycle for a 20-ms pulse envelope. For a 200-ms pulse envelope, the volume of HSP expression using 5% micropulse modulation is reduced to  $5.13 \times 10^{-4} \text{ mm}^3$  from  $6.87 \times 10^{-4} \text{ mm}^3$  at CW.

To understand how temporal modulation affects the calibration challenge for NRT, we use our 577-nm model to calculate the tolerance of the therapeutic window to variation of absorbed power. For simplicity, one can assume that ideal treatment power,  $P_{\text{treatment}}$ , is half between the damage threshold power ( $P_{\text{damage}}$ ) and the HSP expression power ( $P_{\text{HSP}}$ ) to balance the risks of undertreatment and overtreatment. Deviation of the effectively delivered power from ideal, due to variations in ocular transparency and pigmentation, can be expressed as  $\beta = P_{\text{eff}}/P_{\text{treatment}}$ . To avoid tissue damage,  $P_{\text{eff}}$  should not exceed  $P_{\text{damage}}$ , but to trigger therapeutic response,  $P_{\text{eff}}$  should not drop below  $P_{\text{HSP}}$ . Therefore, the therapeutic window for  $\beta$  can be expressed as follows:

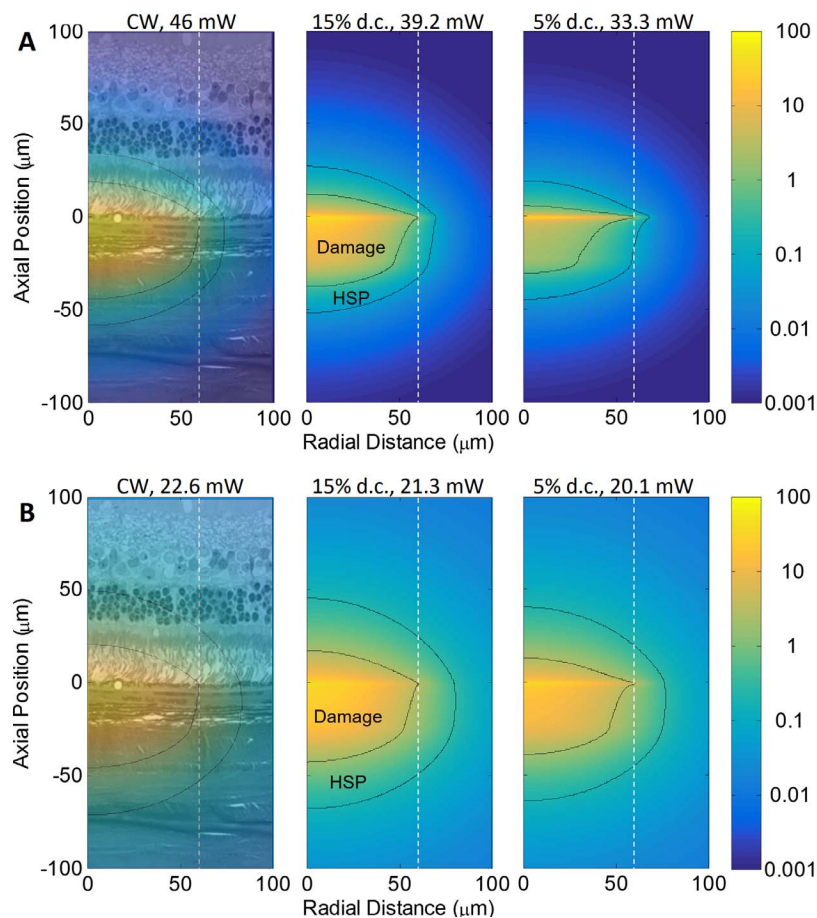
$$P_{\text{HSP}} < P_{\text{eff}} < P_{\text{damage}} \rightarrow \frac{2P_{\text{HSP}}}{P_{\text{damage}} + P_{\text{HSP}}} < \beta < \frac{2P_{\text{damage}}}{P_{\text{damage}} + P_{\text{HSP}}} \quad (2)$$

Figure 8 shows the therapeutic window for CW and 5% micropulse modulation with pulse envelopes from 2 to 200 ms. The therapeutic window is wider at longer pulse durations, and micropulse modulation decreases the therapeutic window across all pulse durations. The variation coefficient  $\beta$  in Figure 8 can be interpreted directly as a change in ocular transparency because it affects the absorbed power linearly. The effect of pigmentation variation is analyzed in Supplementary Figure S1.

## DISCUSSION

### Validity and Limitations of the Arrhenius Model of Tissue Response to Hyperthermia

The in vivo experiments provide many data points to evaluate our thermal model and to test the validity of the Arrhenius integral formulation of tissue response. To account for heat localization at sub-ms pulse durations, we discretized the RPE into a nonpigmented and pigmented layer containing the micrometer-sized melanosomes at the apical surface of the RPE. This change, compared to our previous model of RPE with unstratified pigmentation,<sup>20,29</sup> accentuates the decrease



**FIGURE 6.** Spatial distribution of the Arrhenius integral across the retina and choroid in rabbit model after FA threshold treatment with 577-nm laser in 140- $\mu\text{m}$  spot at the labeled duty cycle and average power for (A) 20-ms and (B) 200-ms pulse envelope. *Black contours* show the range of HSP expression (outside) and cellular damage (inside). *White dotted lines* depict the correlation radius of 60  $\mu\text{m}$  used to translate model to FA threshold in experiment. The *leftmost* image shows rabbit retina overlay.

in computed FA threshold with shorter duty cycle and better matches the corresponding experimental results. At the most extreme micropulse setting, 3% duty cycle and 20-ms pulse envelope, this change yielded a 20% decrease in average power, from 37.6 to 30.2 mW, in computed FA threshold, compared to unstratified RPE cells.

Correlation of the Arrhenius integral values with experimental endpoints shows that this model can predict many effects of temporal modulation reasonably well. The agreement with experimental thresholds down to 5% duty cycle, corresponding to 0.1-ms micropulses, indicates that the Arrhenius integral model successfully portrays tissue response to laser-induced temperature rise down to a 0.1-ms time scale. However, simplification of the thermal denaturation process in biological cells to a single reaction rate with one activation energy has its limits: Arrhenius integral corresponding to the cell damage threshold with 200-ms pulses did not match exactly the threshold integral value observed with 20-ms pulses ( $\Omega_{\text{damage}} = 1$ ), and we had to adjust the  $\Omega_{\text{damage}}$  to 3.04 at 200 ms to better match the experimental data. For a 200-ms pulse, the difference between  $\Omega_{\text{damage}} = 3.04$  and  $\Omega_{\text{damage}} = 1$  corresponds to an 18% increase in final temperature rise, for example, from 17.2°C to 20.8°C at our FA correlation point. Given the complexity of the biological system, including thousands of different proteins, it is not surprising that a single activation energy parameter,  $E^*$ , is insufficient to reproduce precisely the effect of temperature rise over a wide range of pulse durations and peak temperatures. In a previous work by

Takata et al.,<sup>30</sup> a temperature-dependent activation energy was introduced to better fit the data across a wide range of heating parameters, but we chose to keep a single parameter for ease of calculation and use slightly different thresholds for different pulse durations instead.

At the most extreme micropulse condition, 20 ms and 3% duty cycle, our computational model deviated most significantly from the experimental thresholds. The average power of 56.5 mW (experimental threshold for IV lesion) corresponds to calculated peak temperatures as high as 130°C in the RPE—close to an estimated vaporization threshold of 150°C in melanosome.<sup>31</sup> At such short pulse durations ( $\sim 50$   $\mu\text{s}$ ), mechanical damage by vapor bubbles becomes the dominant mechanism, albeit for a single pulse,<sup>32</sup> and hence cellular damage cannot be modeled by Arrhenius integral. Thus, the onset of vaporization limits the use of shorter micropulses to selectively heat the RPE for nondamaging treatment. However, if the goal is to selectively damage the RPE and spare the retina, then nano- to microsecond pulses are the logical choice, as used in selective retina therapy (SRT).<sup>33–35</sup>

While our experiments with rabbit retina allowed comparison of the computational model to various endpoints of tissue damage observed in vivo, we could not utilize it for HSP expression measurements due to the lack of appropriate antibody. Instead, we used a rat model for which there were appropriate antibodies, but this switch may have introduced discrepancies between the model lesion thresholds and

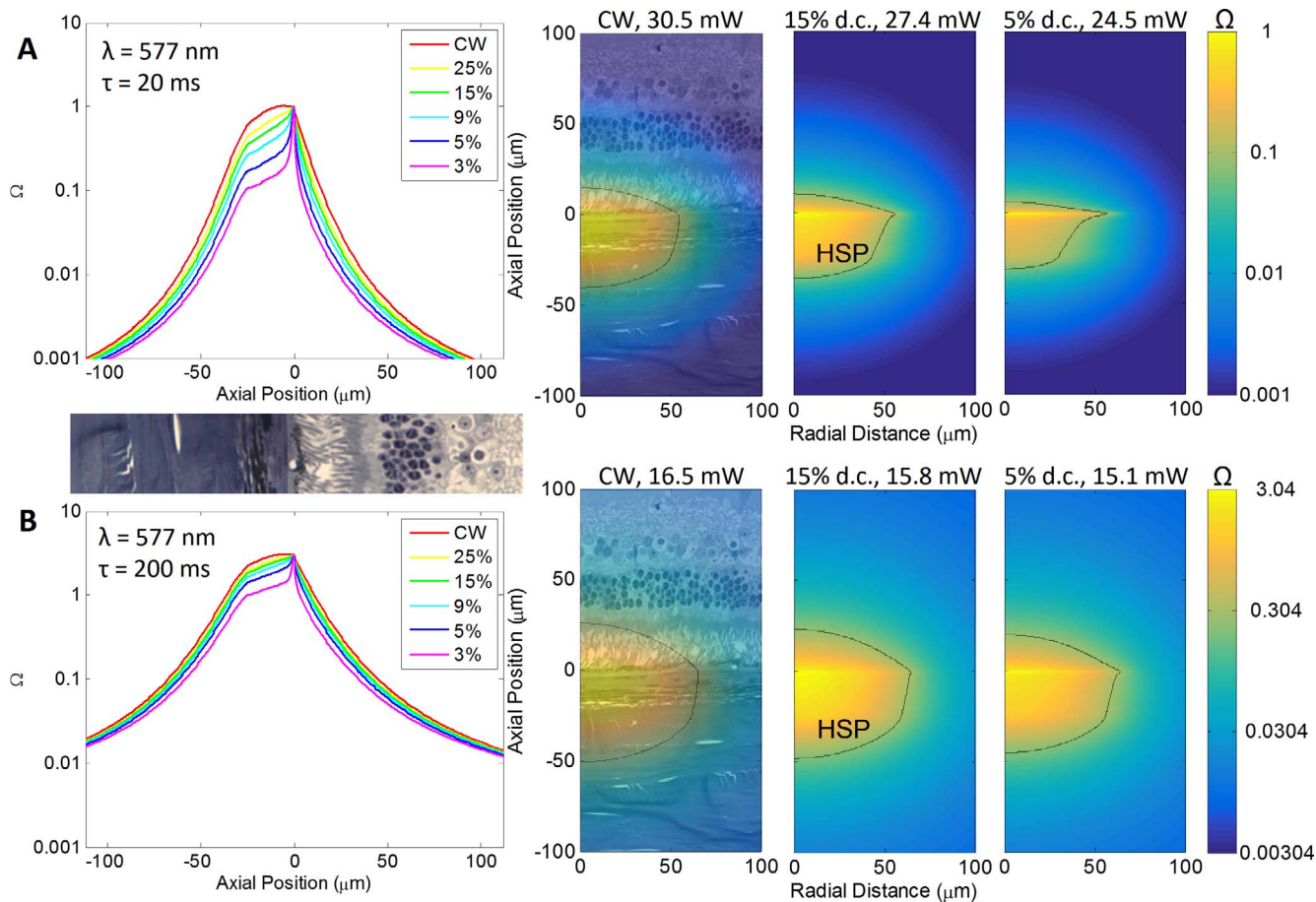


FIGURE 7. Spatial distribution of the Arrhenius integral across the retina and choroid in rabbit model just below damage threshold with 577-nm light in 140- $\mu\text{m}$  spot at the labeled duty cycle and average power for (A) 20-ms and (B) 200-ms pulse envelope. *Black contour* shows the area above the HSP expression threshold. *Plot on the left* shows axial variation of  $\Omega$  at center of the laser beam, with 0 axial position corresponding to the top of the RPE layer, as illustrated with histology of the rabbit retina.

experiments since the retinal and choroidal thicknesses in rats and rabbits are quite different. Thus, to compare model to experiment, we computed the therapeutic window, the ratio of the RPE cell damage power and the HSP expression power, which are both defined by RPE temperature and should be less sensitive to species differences. The therapeutic window from the rabbit model is given in Table 4 next to the experimentally measured values. The agreement between the model and experiment is within the measurement error, which supports our hypothesis that HSP expression can be modeled using the same Arrhenius model parameters as cellular damage. If we assume that HSP expression defines the minimum thermal stress needed for therapeutic effect, then our results reinforce the calibration challenge of NRT. Geeraets et al.<sup>36</sup> estimated the variation between the highest and lowest total absorption at

550 nm in human eyes to be approximately a factor of 2 for the RPE and 3 for the choroid. Such variation exceeds the modeled therapeutic window even at 200 ms, and indicates the importance of titration in each individual. However, even titration in one area cannot compensate for spot-to-spot variation in pigmentation across the retina (e.g., periphery is generally more pigmented than the macula)<sup>37</sup> or retinal scattering due to edema, or transparency variation due to a cataract. The relatively narrow therapeutic window measured here emphasizes significance of the development of methods for real-time temperature monitoring in tissue, such as optoacoustic and optical coherence tomography techniques.<sup>38-40</sup>

One interesting observation made from confocal microscopy was that two layers can express HSP. As shown in Figure 3,

TABLE 4. Therapeutic Window: Ratio of Damage to Onset of Therapeutic Effect. Calculated From Experimental Measurements in Rat, Computational Model for HSP, and for a Hypothetical Lower Therapeutic Threshold

Laser Settings	Damage vs. HSP70 Experiment	HSP Model	Hypothetical Lower Threshold
		$0.1 < \Omega^{20\text{ms}} < 1$ $0.3 < \Omega^{200\text{ms}} < 3$	$0.01 < \Omega^{20\text{ms}} < 1$ $0.03 < \Omega^{200\text{ms}} < 3$
200 ms, CW	$1.36 \pm 0.14$	1.47	2.78
200 ms, 5% duty cycle	$1.40 \pm 0.15$	1.43	2.65
20 ms, CW	$1.39 \pm 0.11$	1.38	2.19
20 ms, 5% duty cycle	$1.30 \pm 0.15$	1.31	1.95

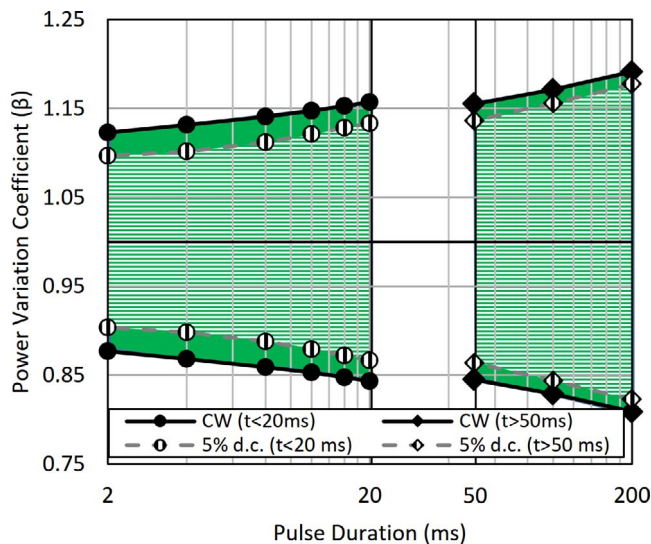


**FIGURE 8.** Tolerance to variation in absorbed power for nondamaging retinal laser therapy. *Markers* indicate maximum power variation before treatment becomes damaging and minimum variation before it becomes subtherapeutic. *Striped markers* indicate laser treatment at 5% duty cycle micropulse modulation and *solid markers* indicate CW treatment. Treatment range was calculated assuming Arrhenius parameters,  $\Omega_{\text{damage}} = 1$  and  $\Omega_{\text{HSP}} = 0.1$  for pulse durations of 2 to 20 ms (shown with *circles*), and  $\Omega_{\text{damage}} = 3.04$  and  $\Omega_{\text{HSP}} = 0.304$  for 50 to 200 ms (shown with *diamonds*).

in addition to RPE, HSP signal can be seen below the Bruch's membrane, most likely in the choriocapillaris. This type of expression was present in both nondamaging and damaging spots at all pulse settings. In contrast, HSP expression in RPE was seen only in the periphery of the damaging burns, regardless of duty cycle. This suggests that cells in choriocapillaris may express HSP at lower threshold than RPE, or that pigmentation in rats is such that choriocapillaris has higher temperature than RPE. The significance of HSP expression for NRT in general, and its location in the retina and choroid, in particular, remain to be explored.

### Effects of a Lower Activation Threshold, Smaller Spot Size, or Longer Wavelength

Although we have used HSP70 expression as the indicator of cellular response to thermal stress, assuming it to be a proxy for therapeutic effect, there may be other pathways for NRT, with different activation thresholds and therapeutic windows. To understand whether such an alternative pathway will change our conclusions, we calculated the therapeutic window for a hypothetical protein expressed at much lower threshold ( $\Omega = \Omega_{\text{HSP}}/10$ ), as shown in the third column of Table 4. If this pathway exists, the therapeutic windows of up to 2.78 may be large enough to tolerate the pigmentation variations

between individuals without titration. However, even in this case, one conclusion remains true: Shorter pulse duration and micropulse modulation only reduce the therapeutic window for nondamaging therapy.

To assess temporal effects, we maintained a fixed laser spot diameter of 140  $\mu\text{m}$ , within the common clinical range of 100 to 210  $\mu\text{m}$  (see Table 5). However, since the spot size affects heat diffusion, it is useful to consider whether our conclusions will change outside this range. First, the therapeutic window, defined as the ratio between RPE damage and HSP expression, is least changed because it is determined by the temperature at the hottest point. Second, as the laser spot diameter decreases below the minimum visible lesion size, the peak temperature required for titration burns increases because heat must diffuse outward to the visible diameter. As a result, the RPE damage threshold, measured in the center of the lesion, becomes a smaller percentage of the titration threshold. Finally, micropulse modulation in smaller spots results in larger deviation in threshold power from CW laser because the heat diffuses away more completely within the micropulse period. For the standard micropulse period of 2 ms, the thermal diffusion length,  $L = \sqrt{4\kappa t}$ , is 33  $\mu\text{m}$ .<sup>41</sup> Thus, as shown in Supplementary Figure S2, heat can readily diffuse away from 20- $\mu\text{m}$ -diameter spots, while it accumulates in larger spots (140-, 200- $\mu\text{m}$  diameters).

While we did not use an infrared laser in our experimental measurements, the effect of longer wavelengths, such as 810 nm, can also be assessed using computational model. Due to the reduced absorption in melanin, more light penetrates to the choroid, making both HSP expression and damage more likely in the choroid, especially with longer pulse envelopes (see Supplementary Figs. S3, S4). Conversely, the retinal temperature profile and tissue response are very similar between 577 and 810 nm.

### Comparison of the Model to Clinical Settings

The Arrhenius model calibrated in this study can be used for comparison of various treatment protocols involving different duty cycles and calibration algorithms. We analyzed several published clinical reports based on 577-nm laser, where a titration protocol based on visible damage was described. First, the specified titration power was set as the IV threshold in our model for the spot size and pulse duration in the study. Then, the Arrhenius integral was calculated for the treatment parameters. For example, the Supra Scan 577 nm (Quantel Medical, Courmon d'Auvergne, France) treatment protocol advises titrating with 5% duty cycle and 200-ms pulse envelope with a 150- $\mu\text{m}$  retinal spot, and then treating at half the titration power.<sup>42</sup> This corresponds to a maximum  $\Omega = 4.1$  (Table 5), which is slightly above the damage threshold in our model ( $\Omega_{\text{damage}} = 3.04$ ). If titration is performed in a nonedematous periphery and treatment is applied to the diseased macula, the absorbed laser power in the treatment areas is likely to be less than in the titration zone. Therefore, this treatment is likely to be just below the damage threshold

**TABLE 5.** Comparison of Clinical Settings. NRT Range Is Expected to be  $0.3 < \Omega_{200\text{ms}} < 3$

Study	$\lambda$ , nm	Spot, $\mu\text{m}$	Titration	Treatment Power	Duration, ms	Duty Cycle	Arrhenius $\Omega$
Quantel SupraScan 577 <sup>42</sup>	577	150	5% duty cycle, 200 ms	50% titration	200	5%	4.1
Quantel for macular edema <sup>43</sup>	577	110	CW, 200 ms	200% titration	200	15%/9%	0.63/0.065
Yadav et al., 2015 <sup>8</sup>	577	100	CW, 200 ms	50% titration	200	10%	0.007
Luttrull et al., 2012 <sup>7</sup>	810	131	NA	950 mW	300	5%	0.43
Luttrull, Margolis, 2016 <sup>44</sup>	810	210	NA	1400 mW	150	5%	0.10
Vujosevic et al., 2010 <sup>45</sup>	810	125	NA	750 mW	200	5%	0.09

and well above the HSP threshold of 0.3. Another study with 577-nm, 200-ms laser used titration to visible lesion with CW and treatment with twice the power at either 15% or 9% duty cycle, all with 100- to 120- $\mu\text{m}$  (110- $\mu\text{m}$  for modeling) spots.<sup>43</sup> For these settings,  $\Omega = 0.63$  is in the NRT range for 15% duty cycle, but only  $\Omega = 0.065$  for 9% duty cycle, which is below our HSP threshold. In a third study, which used treatment at 10% duty cycle and half the CW titration power in a 100- $\mu\text{m}$  spot, the maximum  $\Omega = 0.0078$ —two orders of magnitude below the expected therapeutic range.

We also calculated Arrhenius values for 810-nm treatments, where no titration is done, and tabulated the results in Table 5. Assuming the patient's optical characteristics match model parameters in Table 2, treatment using laser settings from Luttrull et al.<sup>7</sup> yields  $\Omega$  within the expected range for nondamaging treatment, but two other settings<sup>44,45</sup> produce Arrhenius values below  $\Omega_{\text{HSP}} = 0.3$ . In addition, without titration, variations in pigmentation and transparency could produce widely varying results in different patients. For each of these micropulse treatment protocols, similar Arrhenius values can be achieved using CW laser with 105% of the average power (peak power multiplied by duty cycle) while keeping the same spot size, wavelength, and pulse duration. As a whole, the small Arrhenius values corresponding to laser settings in these studies suggest either that therapeutic response begins below the HSP expression threshold, or that some treatment protocols would benefit from higher settings.

Since NRT involves application of hundreds of laser exposures, it is very tedious if performed manually spot by spot, and invisible spots are difficult to align for uniform coverage. Pattern scanning, especially with automatic advancement, and with alignment relative to the fovea can solve both problems.<sup>4</sup> However, for more than 10 spots in the pattern to be applied sequentially during the eye fixation time, each exposure should not exceed approximately 20 ms. While shorter exposures reduce the total treatment time in pattern scanning and limit unpredictable spot spreading due to eye movements (up to 0.9  $\mu\text{m}/\text{ms}$ ),<sup>46</sup> they also decrease the therapeutic window. If the treatment aim is solely to avoid neuroretinal damage, shorter pulse durations and duty cycles help localize the thermal stress to the RPE and hence are preferable. However, if the treatment mandates no damage to any cell layer, such as NRT, reduced spread of heat with shorter pulses and with micropulse modulation is not beneficial, and maybe even detrimental since it decreases the volume of tissue exposed to therapeutic level of thermal stress.

## CONCLUSIONS

Micropulse modulation with sufficiently short envelope and duty cycle reduces the spread of heat from the light-absorbing RPE and choroid. However, this heat localization does not benefit the NRT. Rather, it only decreases the treated volume and diminishes the therapeutic window.

## Acknowledgments

The authors thank Anthony Mo and Michelle Shao of Topcon Medical Laser Systems for assistance with laser modulation and software, Philip Huie for assistance with development of immunofluorescence protocols, Henri Lorach for assistance with confocal imaging, and Daniel Lavinsky for helpful discussions. We also thank the Stanford Cell Sciences Imaging Facility for use of the Zeiss LSM 780 confocal microscope.

Supported, in part, by the Stanford Photonics Research Center.

Disclosure: **J. Wang**, None; **Y. Quan**, None; **R. Dalal**, None; **D. Palanker**, Topcon Medical Laser Systems (C, F), P

## References

- Lavinsky D, Cardillo JA, Melo LAS, Dare A, Farah ME, Belfort R. Randomized clinical trial evaluating mETDRS versus normal or high-density micropulse photocoagulation for diabetic macular edema. *Invest Ophthalmol Vis Sci*. 2011;52:4314-4323.
- Luttrull JK, Dorin G. Subthreshold diode micropulse laser photocoagulation (SDM) as invisible retinal phototherapy for diabetic macular edema: a review. *Curr Diabetes Rev*. 2012;8:274-284.
- Lavinsky D, Palanker D. Nondamaging photothermal therapy for the retina. *Retina*. 2015;35:213-222.
- Lavinsky D, Wang J, Huie P, et al. Nondamaging retinal laser therapy: rationale and applications to the macula. *Invest Ophthalmol Vis Sci*. 2016;57:2488-2500.
- Luttrull JK, Chang DB, Margolis BWL, Dorin G, Luttrull DK. Laser resensitization of medically unresponsive neovascular age-related macular degeneration. *Retina*. 2015;35:1184-1194.
- Lavinsky D, Sramek C, Wang J, et al. Subvisible retinal laser therapy: titration algorithm and tissue response. *Retina*. 2014;34:87-97.
- Luttrull JK, Sramek C, Palanker D, Spink CJ, Musch DC. Long-term safety, high-resolution imaging, and tissue temperature modeling of subvisible diode micropulse photocoagulation for retinovascular macular edema. *Retina*. 2012;32:375-386.
- Yadav NK, Jayadev C, Mohan A, et al. Subthreshold micropulse yellow laser (577 nm) in chronic central serous chorioretinopathy: safety profile and treatment outcome. *Eye*. 2015;29:258-264, quiz 265.
- Kwon YH, Lee DK, Kwon OW. The short-term efficacy of subthreshold micropulse yellow (577-nm) laser photocoagulation for diabetic macular edema. *Korean J Ophthalmol*. 2014;28:379.
- Mainster MA. Decreasing retinal photocoagulation damage: principles and techniques. *Semin Ophthalmol*. 1999;14:200-209.
- Figueira J, Khan J, Nunes S, et al. Prospective randomised controlled trial comparing sub-threshold micropulse diode laser photocoagulation and conventional green laser for clinically significant diabetic macular oedema. *Br J Ophthalmol*. 2009;93:1341-1344.
- Venkatesh P, Ramanjulu R, Azad R, Vohra R, Garg S. Subthreshold micropulse diode laser and double frequency neodymium: YAG laser in treatment of diabetic macular edema: a prospective, randomized study using multifocal electroretinography. *Photomed Laser Surg*. 2011;29:727-733.
- Sivaprasad S, Elagouz M, McHugh D, Shona O, Dorin G. Micropulsed diode laser therapy: evolution and clinical applications. *Surv Ophthalmol*. 2010;55:516-530.
- Abouhoussein MA. Micropulse laser for diabetic macular edema. *Delta J Ophthalmol*. 2016;17:167.
- Jean M, Schulmeister K. Modeling of laser-induced thermal damage to the retina and the cornea. In: Ng EYK, Acharya UR, Campilho A, Suri JS, eds. *Image Analysis and Modeling in Ophthalmology*. Boca Raton, FL: CRC Press; 2014:265-292.
- Birngruber R, Hillenkamp F, Gabel VP. Theoretical investigations of laser thermal retinal injury. *Health Phys*. 1985;48:781-796.
- Henriques FC. Studies of thermal injury; the predictability and the significance of thermally induced rate processes leading to irreversible epidermal injury. *Arch Pathol*. 1947;43:489-502.

18. Lepock JR. Cellular effects of hyperthermia: relevance to the minimum dose for thermal damage. *Int J Hyperthermia*. 2003;19:252-266.
19. Morimoto RI. Regulation of the heat shock transcriptional response: cross talk between a family of heat shock factors, molecular chaperones, and negative regulators. *Genes Dev*. 1998;12:3788-3796.
20. Sramek C, Paulus Y, Nomoto H, Huie P, Brown J, Palanker D. Dynamics of retinal photocoagulation and rupture. *J Biomed Opt*. 2009;14:34007.
21. Sramek C, Mackanos M, Spittler R, et al. Non-damaging retinal phototherapy: dynamic range of heat shock protein expression. *Invest Ophthalmol Vis Sci*. 2011;52:1780-1787.
22. Wang L, Jacques SL, Zheng L. MCML—Monte Carlo modeling of light transport in multi-layered tissues. *Comput Methods Programs Biomed*. 1995;47:131-146.
23. Wang L, Jacques SL, Zheng L. CONV-convolution for responses to a finite diameter photon beam incident on multi-layered tissues. *Comput Methods Programs Biomed*. 1997;54:141-150.
24. Kim IT, Choi JB. Melanosomes of retinal pigment epithelium—distribution, shape, and acid phosphatase activity. *Korean J Ophthalmol*. 1998;12:85-91.
25. Song WK, Lee SC, Lee ES, Kim CY, Kim SS. Macular thickness variations with sex, age, and axial length in healthy subjects: a spectral domain-optical coherence tomography study. *Invest Ophthalmol Vis Sci*. 2010;51:3913-3918.
26. Ruiz-Moreno JM, Flores-Moreno I, Lugo F, Ruiz-Medrano J, Montero JA, Akiba M. Macular choroidal thickness in normal pediatric population measured by swept-source optical coherence tomography. *Invest Ophthalmol Vis Sci*. 2013;54:353-359.
27. Grunwald GB. Structure and function of the retinal pigment epithelium. In: *Duane's Foundations of Clinical Ophthalmology*. Vol. 1. Philadelphia: Lippincott Williams & Wilkins; 2006.
28. Hammer M, Roggan A, Schweitzer D, Müller G. Optical properties of ocular fundus tissues—an in vitro study using the double-integrating-sphere technique and inverse Monte Carlo simulation. *Phys Med Biol*. 1995;40:963-978.
29. Sramek CK, Leung L-SB, Paulus YM, Palanker DV. Therapeutic window of retinal photocoagulation with green (532-nm) and yellow (577-nm) lasers. *Ophthalmic Surg Lasers Imaging*. 2012;43:341-347.
30. Takata A, Zaneveld L, Richter W. Laser-induced thermal damage of skin. In: *Report SAM-TR-77-38*. USAF School of Aerospace Medicine; 1977:1-159.
31. Brinkmann R, Hüttmann G, Rögner J, Roeder J, Birngruber R, Lin CP. Origin of retinal pigment epithelium cell damage by pulsed laser irradiance in the nanosecond to microsecond time regimen. *Lasers Surg Med*. 2000;27:451-464.
32. Schuele G, Rumohr M, Huettmann G, Brinkmann R. RPE damage thresholds and mechanisms for laser exposure in the microsecond-to-millisecond time regimen. *Invest Ophthalmol Vis Sci*. 2005;46:714-719.
33. Brinkmann R, Roeder J, Birngruber R. Selective retina therapy (SRT): a review on methods, techniques, preclinical and first clinical results. *Bull Soc Belge Ophthalmol*. 2006;302:51-69.
34. Roeder J, Liew SHM, Klatt C, et al. Selective retina therapy (SRT) for clinically significant diabetic macular edema. *Graefes Arch Clin Exp Ophthalmol*. 2010;248:1263-1272.
35. Wood JPM, Shibebe O, Plunkett M, Casson RJ, Chidlow G. Retinal damage profiles and neuronal effects of laser treatment: comparison of a conventional photocoagulator and a novel 3-nanosecond pulse laser. *Invest Ophthalmol Vis Sci*. 2013;54:2305-2318.
36. Geeraets WJ, Williams RC, Chan G, et al. The relative absorption of thermal energy in retina and choroid. *Invest Ophthalmol Vis Sci*. 1962;1:340-347.
37. Schmidt SY, Peisch RD. Melanin concentration in normal human retinal pigment epithelium. Regional variation and age-related reduction. *Invest Ophthalmol Vis Sci*. 1986;27:1063-1067.
38. Müller HH, Ptaszynski L, Schlott K, et al. Imaging thermal expansion and retinal tissue changes during photocoagulation by high speed OCT. *Biomed Opt Express*. 2012;3:1025.
39. Kandulla J, Elsner H, Birngruber R, Brinkmann R. Noninvasive optoacoustic online retinal temperature determination during continuous-wave laser irradiation. *J Biomed Opt*. 2006;11:41111.
40. Brinkmann R, Koinzer S, Schlott K, et al. Real-time temperature determination during retinal photocoagulation on patients. *J Biomed Opt*. 2012;17:61219.
41. Niemz MH. *Laser-Tissue Interactions: Fundamentals and Applications*. Berlin: Springer; 2004.
42. Chong V. Micropulse treatment guidelines. Available at: [http://www.retina-yellow-laser-therapy.com/assets/superscan.treatment-guidelines.subliminal.xl\\_supscan577subliminal\\_ms\\_anfr\\_170522.pdf](http://www.retina-yellow-laser-therapy.com/assets/superscan.treatment-guidelines.subliminal.xl_supscan577subliminal_ms_anfr_170522.pdf). Accessed May 11, 2016.
43. Hamon F, Soyeur R. Micropulse laser for macular edema. Available at: <http://www.quantel-medical.com/products/download/112/en>. Accessed January 9, 2017.
44. Luttrull JK, Margolis BWL. Functionally guided retinal protective therapy for dry age-related macular and inherited retinal degenerations: a pilot study. *Invest Ophthalmol Vis Sci*. 2016;57:265-275.
45. Vujosevic S, Bottega E, Casciano M, Pilotto E, Convento E, Midena E. Microperimetry and fundus autofluorescence in diabetic macular edema: subthreshold micropulse diode laser versus modified early treatment diabetic retinopathy study laser photocoagulation. *Retina*. 2010;30:908-916.
46. Poletti M, Listorti C, Rucci M. Stability of the visual world during eye drift. *J Neurosci*. 2010;30:11143-11150.